Technical Supplementary Information: In silico trials predict that combination strategies for enhancing vesicular stomatitis oncolytic virus are determined by tumour aggressivity

Authors: Adrianne L. Jenner, Tyler Cassidy, Katia Belaid, Marie-Claude Bourgeois-Daigneault, Morgan Craig

Correspondence to :

morgan.craig@umontreal.ca

This PDF file includes:

Methods

Supplementary Analysis

Figs. TS1 to TS4

Tables S1 to S3

References 1 to 14

Jenner AL, *et al. J Immunother Cancer* 2021; 9:e001387. doi: 10.1136/jitc-2020-001387

METHODS

Mathematical model of combination OV-based therapeutic vaccination

The computational model's formalism was based on Cassidy and Humphries[1], with parameterization as in Cassidy and Craig[2], who determined optimized treatment schedules for combined T-VEC and GM-CSF. This model explicitly accounts for heterogeneity in tumour cell cycle time and tumour-immune interactions through a distributed delay differential equation, and describes the quiescent tumour cell population ($Q(t)$), and the G1-phase tumour cell population ($G_1(t)$) with the remainder of mitosis described as a delayed process with a delay kernel $K(t)$ representing the duration of the mitotic portion of the cell cycle. We assumed that the cell cycle duration is Erlang distributed as was done by Cassidy and Craig[2], but other distributions are also possible[1,3,4].

As described in the main text, we have expanded the model described in Cassidy and Craig[2] to include vaccinia (VV) and vesicular stomatitis virus (VSV) viral strains, $V_{VV}(t)$ and $V_{VSV}(t)$, and associated viral dynamics. This includes the introduction of virus-specific rates for the virion to cell infection rate, κ_{VSV} and κ_{VV}; the cell lysis rate, δ_{VSV} and δ_{VV}; the lytic virion burst size, α_{VSV} and α_{VV}; and the virion death rate, ω_{VSV} and ω_{VV}. Similarly, the model now includes a VV-infected cell population, $I_{VV}(t)$, and a VSV-infected cell population, $I_{VSV}(t)$. Pro-inflammatory cytokines, $C(t)$, are produced in response to the presence of uninfected and infected tumour cells. Immune cells, $P(t)$, are recruited to the tumour site by the cytokine concentration and are able to kill uninfected tumour cells. We consider $P(t)$ to represent the overall average response of the immune system and includes the action of macrophages, T cells and other phagocytes. The complete model is given by

$$\frac{d}{dt}Q(t) = 2(1-\mu)\int_{-\infty}^{t} exp\left[-\int_{\sigma}^{t}\hat{d}_K + \kappa_{VV}\eta\big(V_{VV}(x)\big) + \kappa_{VSV}\eta\big(V_{VSV}(x)\big) + \psi_G\big(U(x)\big)dx\right] a_2 G_1(\sigma)K(t - \sigma)d\sigma - \big[a_1 + d_1 + \psi_Q\big(U(t)\big)\big]Q(t)$$

$$\frac{d}{dt}G_1(t) = a_1 Q(t) - \big[a_2 + d_2 + \kappa_{VV}\eta\big(V_{VV}(t)\big) + \kappa_{VSV}\eta\big(V_{VSV}(t)\big) + \psi_G\big(U(t)\big)\big]G_1(t),$$

$$\frac{d}{dt}Q_R(t) = 2\mu\int_{-\infty}^{t}\exp\left[-\int_{\sigma}^{t}\hat{d}_K + \kappa_{VV}\eta\big(V_{VV}(x)\big) + \kappa_{VSV}\eta\big(V_{VSV}(x)\big) + \psi_G\big(U(x)\big)dx\right]a_2G_1(\sigma)K(t-\sigma)d\sigma$$

$$+\ 2\int_{-\infty}^{t}\exp\left[-\int_{\sigma}^{t}\hat{d}_K + \kappa_{VV}\eta\big(V_{VV}(x)\big) + \kappa_{VSV}\eta\big(V_{VSV}(x)\big)dx\right]a_2G_{1,R}(\sigma)K(t-\sigma)d\sigma$$

$$-\ [a_1 + d_1]Q_R(t),$$

$$\frac{d}{dt}G_{1,R}(t) = a_1Q_R(t) - \big[a_2 + d_2 + \kappa_{VV}\eta\big(V_{VV}(t)\big) + \kappa_{VSV}\eta\big(V_{VSV}(t)\big)\big]G_{1,R}(t),$$

$$\frac{d}{dt}I_{VSV}(t) = \kappa_{VSV}\eta\big(V_{VSV}(t)\big)\big[G_1(t) + G_{1,R}(t) + N(t) + N_R(t)\big] - \delta_{VSV}I_{VSV}(t),$$

$$\frac{d}{dt}I_{VV}(t) = \kappa_{VV}\eta\big(V_{VV}(t)\big)\big[G_1(t) + G_{1,R}(t) + N(t) + N_R(t)\big] - \delta_{VV}I_{VV}(t),$$

$$\frac{d}{dt}V_{VSV}(t) = -\kappa_{VSV}\eta\big(V_{VSV}(t)\big)\big[G_1(t) + G_{1,R}(t) + N(t) + N_R(t)\big] + \alpha_{VSV}\delta_{VSV}I_{VSV}(t) - \omega_{VSV}V_{VSV}(t),$$

$$\frac{d}{dt}V_{VV}(t) = -\kappa_{VV}\eta\big(V_{VV}(t)\big)\big[G_1(t) + G_{1,R}(t) + N(t) + N_R(t)\big] + \alpha_{VV}\delta_{VV}I_{VV}(t) - \omega_{VV}V_{VV}(t),$$

$$\frac{d}{dt}C(t) = C_{prod}\big(U(t)\big) - k_{elim}C(t),$$

$$\frac{d}{dt}P(t) = \phi\big(C(t)\big) - \gamma_pP(t),$$

$$I(t) = I_{VSV}(t) + I_{VV}(t),$$

$$V(t) = V_{VSV}(t) + V_{VV}(t).$$

All other parameters are in Cassidy and Craig[2]. To simplify notation in the functions $\eta\big(U(t)\big), \psi_Q\big(U(t)\big), \psi_G\big(U(t)\big), \phi\big(C(t)\big)$, and $C_{prod}\big(U(t)\big)$ described below, we introduce

$$U(t) = [Q(t), G_1(t), I(t), V(t), C(t), P(t)].$$

Phagocytosis of quiescent and mitotic tumour cells was considered to occur at respective rates

$$\psi_Q\big(U(t)\big)Q(t) = \frac{k_pP(t)}{1+k_QQ(t)}Q(t),$$

and

$$\psi_G\big(U(t)\big)G_1(t) = \frac{k_pP(t)}{1+k_sG_1(t)}G_1(t).$$

The infection of susceptible cells by the oncolytic virus was modelled by

$$\eta\big(V(t)\big) = \frac{V(t)}{\eta_{1/2} + V(t)}.$$

Immune cells are recruited to the tumour microenvironment by the inflammatory cytokines at a rate of

$$\phi\big(C(t)\big) = \frac{k_{cp}C(t)}{C_{1/2}+C(t)},$$

and inflammatory cytokines are produced at rate

$$C_{prod}\big(U(t)\big) = C^*_{prod} + \rho\big(C^{max}_{prod} - C^*_{prod}\big)\frac{\delta I + \Psi\big(U(t)\big)}{\Psi_{\frac{1}{2}} + \delta I + \Psi\big(U(t)\big)},$$

where

$$\Psi\big(U(t)\big) = \psi_G(P, G_1)G_1 + \psi_Q(P, Q)Q = \frac{k_p P(t)}{1 + k_s G_1(t)}(G_1(t) + N(t)) + \frac{k_p P(t)}{1 + k_q Q(t)}Q(t).$$

An anti-inflammatory state can be caused by cells releasing anti-inflammatory cytokines such as interleukin-10 (IL-10) or transforming growth factor β (TGF-β)[5] after viral infection. Further, infection by virus can also cause a reduction in the production of pro-inflammatory cytokines, e.g. interleukin-12 (IL-12), that are necessary to support a strong anti-viral immune response[5]. In contrast, a pro- inflammatory response is instigated when a virus-infected cell activates immune cells through cytokine signaling. These activated immune cells release pro-inflammatory immune-stimulatory cytokines, such as IL-12 and IL-2[6–8], that aid in the recruitment and proliferation of immune cells. The ability of viruses to instigate a pro- or anti-inflammatory immune response depends on the type of virus. As mentioned in the main text, to model the immune response, we introduced an inflammatory modulation parameter (ρ) into the production rate of inflammatory cytokines $C_{prod}\big(U(t)\big)$ where $0 \leq \rho \leq 1$. Cytokine production from infected cells and cycling tumour cells is decreased for small values of ρ, simulating an anti-inflammatory response.

The total number of non-resistant and resistant cells in the cell cycle, $N(t)$ and $N_R(t)$ respectively, is thus given by

$$N(t) = \int_0^\infty a_2 \exp\left[-\int_{t-\xi}^{t} \hat{d}_K + \kappa_{VV}\eta\big(V_{VV}(x)\big) + \kappa_{VSV}\eta\big(V_{VSV}(x)\big) + \psi_G\big(U(x)\big)dx\right]\Bigg(1 - \int_0^\xi K(\sigma)d\sigma\Bigg)\, G_1(t-\xi)d\xi,$$

and

$$N_R(t) = \int_0^\infty a_2 \exp\left[-\int_{t-\xi}^{t} \hat{d}_K + \kappa_{VV}\eta\big(V_{VV}(x)\big) + \kappa_{VSV}\eta\big(V_{VSV}(x)\big)dx\right]\left(1 - \int_0^\xi K(\sigma)d\sigma\right) G_{1,R}(t-\xi)\, d\xi.$$

The total number of tumour cells $T(t)$ at any point in time t is calculated by

$$T(t) = Q(t) + G_1(t) + N(t) + Q_R(t) + G_{1,R}(t) + N_R(t) + I_{VV}(t) + I_{VSV}(t).$$

Intravenous administration of oncolytic viruses was modelled by

$$Dose_V(t) = \sum_{j=1}^{N} \frac{k_a^v F_v Admin_i^v(t)}{Vol} \exp\left(-k_a^v\big(t - t_j\big)\right),$$

where $Dose_j^v$ is the amount of virus administered at time $t = t_j$ and

$$Admin_j^v(t) = \begin{cases} 0 & if\ t < t_j, \\ Dose_j^v & if\ t \geq t_j, \end{cases}$$

similar to the formalism in Cassidy and Craig[2].

To numerically solve the full model, we applied the linear chain technique to replace the distributed delay term by the solution of a system of linear ODEs and reduce the system to an equivalent finite dimensional system of ODEs[1–3]. This reduction now explicitly depends on the shape and scale parameters, k_{tr} and j, that arise from the parametrization of the Erlang distribution kernel $K(t)$[2]. The transformed system of ODEs is given by

$$\frac{dQ(t)}{dt} = \ 2(1-\mu)k_{tr}A_j(t) - a_1Q(t) - d_1Q(t) - \psi_Q\big(U(t)\big)Q(t),$$

$$\frac{dG_1(t)}{dt} = a_1Q(t) - \left[a_2 + d_2 + \kappa_{VV}\eta\big(V_{VV}(t)\big) + \kappa_{VSV}\eta\big(V_{VSV}(t)\big) + \psi_{_G}\big(U(t)\big)\right]G_1(t),$$

$$\frac{dA_1(t)}{dt} = a_2G_1(t) - k_{tr}A_1(t) - \left(\hat{d}_g + \kappa_{VV}\eta\big(V_{VV}(t)\big) + \kappa_{VSV}\eta\big(V_{VSV}(t)\big) + \psi_G\big(U(t)\big)\right)A_1(t),$$

$$\frac{dA_i(t)}{dt} = k_{tr}\big(A_{i-1}(t) - A_i(t)\big) - \left(\hat{d}_g + \kappa_{VV}\eta\big(V_{VV}(t)\big) + \kappa_{VSV}\eta\big(V_{VSV}(t)\big) + \psi_G\big(U(t)\big)\right)A_i(t),$$

$$\text{for } i = 2,3,\dots,j$$

$$\frac{dQ_R(t)}{dt} = 2\mu k_{tr}A_j(t) + 2k_{tr}A_{j,R}(t) - a_1Q_R(t) - d_1Q_R(t),$$

$$\frac{dG_{1,R}(t)}{dt} = a_1Q_R(t) - a_2G_{1,R}(t) - d_2G_{1,R}(t) - (\kappa_{VV}\eta\big(V_{VV}(t)\big) + \kappa_{VSV}\eta\big(V_{VSV}(t)\big)\,)G_{1,R}(t),$$

$$\frac{dA_{1,R}(t)}{dt} = a_2 G_{1,R}(t) - k_{tr} A_{1,R}(t) - \left(\hat{d}_g + \kappa_{VV}\eta\left(V_{VV}(t)\right) + \kappa_{VSV}\eta\left(V_{VSV}(t)\right) + \psi_G\left(U(t)\right)\right) A_{1,R}(t),$$

$$\frac{dA_{i,R}(t)}{dt} = k_{tr}\left(A_{i-1,R}(t) - A_{i,R}(t)\right) - \left(\hat{d}_g + \kappa_{VV}\eta\left(V_{VV}(t)\right) + \kappa_{VSV}\eta\left(V_{VSV}(t)\right) + \psi_G\left(U(t)\right)\right) A_{i,R}(t),$$

$$\text{for } i = 2,3,\ldots,j,$$

$$\frac{dI_{VV}(t)}{dt} = \kappa_{VV}\eta\left(V_{VV}(t)\right)\left[G_1(t) + G_{1,R}(t) + N(t) + N_R(t)\right] - \delta_{VV} I_{VV}(t),$$

$$\frac{dI_{VSV}(t)}{dt} = \kappa_{VSV}\eta\left(V_{VSV}(t)\right)\left[G_1(t) + G_{1,R}(t) + N(t) + N_R(t)\right] - \delta_{VSV} I_{VSV}(t),$$

$$\frac{dV_{VV}(t)}{dt} = \alpha_{VV}\delta_{VV} I_{VV}(t) - \omega_{VV} V_{VV}(t) - \kappa_{VV}\eta\left(V_{VV}(t)\right)\left(G_1(t) + N(t)\right),$$

$$\frac{dV_{VSV}(t)}{dt} = \alpha_{VSV}\delta_{VSV} I_{VSV}(t) - \omega_{VSV} V_{VSV}(t) - \kappa_{VSV}\eta\left(V_{VSV}(t)\right)\left(G_1(t) + N(t)\right),$$

$$\frac{dC(t)}{dt} = C_{prod}\left(U(t)\right) - k_{elim} C(t),$$

$$\frac{dP(t)}{dt} = \phi\left(C(t)\right) - \gamma_p P(t)$$

with initial conditions carefully chosen to ensure that the solution of the finite dimensional system above defined a solution of the infinite dimensional distributed DDE model[1,2]. The initial conditions for the cytokine and immune cells (C_0 and P_0 respectively) were determined by solving P and C at homeostasis, i.e. setting $dP/dt = dC/dt = 0$. The variables in the model are summarized in Table TS1, with values obtained during fitting in Table TS2 and then final parameter values in Table TS3-TS4.

Parameter	Units	Description
$Q(t)$	cells	Quiescent tumour cells
$G_1(t)$	cells	G1-phase tumour cells
$Q_R(t)$	cells	Resistant quiescent tumour cells
$G_{1,R}(t)$	cells	Resistant G1-phase tumour cells
$I_{VSV}(t)$	cells	Tumour cells infected by VSV
$I_{VV}(t)$	cells	Tumour cells infected by VV
$I(t)$	cells	Total infected cell population
$V_{VSV}(t)$	virions	Vesicular stomatitis virus (VSV) free virus
$V_{VV}(t)$	virions	Vaccinia (VV) free virus
$V(t)$	virions	Total virus
$C(t)$	ng/mL	Cytokine concentration
$P(t)$	10^{10}cells	Immune cells
$N(t)$	Cells	The total number of non-resistant tumour cells in the cell cycle
$N_R(t)$	Cells	The total number of resistant tumour cells in the cell cycle

Table TS1. Summary of variables in the model.

Experimental measurements used to estimate VV and VSV related viral and immune parameters

To estimate the parameters in the model, we used a hierarchical fitting algorithm where subsets of the model were fit to different experiments using VV and VSV in immunodeficient and immunocompetent mice to allow for individual aspects of a given biological interaction to be understood in isolation. For example, we leveraged experiments in immunodeficient mice to fit parameters in the model relating solely to tumour growth. These parameters were then fixed when fitting the immune-related parameters to data from immunocompetent mice. Using this approach, we reduce the degrees of freedom at each stage of parameter fitting and obtain more reliable estimates for individual parameter values.

Two primary data sources were leveraged. Le Boeuf *et al.*[9] measured the relative tumour volume in immunodeficient and immunocompetent mice after treatment with VV and VSV. Tumours were established using the HT29 (human colorectal adenocarcinoma) cell line in immunodeficient mice with an initial injection of 3×10^6 cells. After 10 days, they tested three treatment protocols on the these tumours: a single intravenous injection of VSV (1×10^7pfu), a single intravenous injection of VV (1×10^6 pfu), and a single intravenous injection of VV (1×10^6 pfu) followed two days later by a single intravenous injection of VSV (1×10^7pfu). Cell line 4T1 (breast cancer) tumours were then established in immunocompetent mice using an initial injection of 1×10^5 cells. After 6 days, they tested three treatment protocols: using a single intravenous injection of VSV (1×10^8 pfu), a single intravenous injection of VV (1×10^7 pfu), and a single intravenous injection of VV (1×10^7pfu) followed two days later by a single intravenous injection of VSV (1×10^8 pfu). The relative tumour volume $\tilde{T}(t, \hat{t})$ on day t relative to day $\hat{t}$ i.e.

$$\tilde{T}(t, \hat{t}) = \frac{T(t) - T(\hat{t})}{T(\hat{t})} \times 100, \qquad (1)$$

was monitored for ten mice in each protocol for each cell line and then averaged for each experiment. In Eq. (1), $T(t)$ is the tumour volume on day t, and is used to calculate the relative tumour volume $\tilde{T}(t, \hat{t})$, also known also as a relative index[10,11].

We also incorporated 4T1 tumour growth measurements in immunodeficient and immunocompetent mice from Rausch *et al.*[12]. Here, tumour growth was reported in area (mm^2) as opposed to in volume (mm^3) as in Le Boeuf *et al*. We therefore converted Rausch *et al.*'s tumour area measurements to tumour volume by assuming the tumours were spherical. We also converted both sets of data to a measurement for the number of cells by assuming that 1 mm^3 contains 1×10^6cells[2,13]. The nine experiments considered are summarized below:

- *HT29/ID* - HT29 cell tumour growth in an immune-deficient mouse model
- *4T1/ID* – 4T1 cell tumour growth in an immune-deficient mouse model
- *HT29/ID-VSV* – HT29 cell tumour growth under VSV treatment in immune-deficient mouse model
- *HT29/ID-VV* – HT29 cell tumour growth under VV treatment in immune-deficient mouse model
- *HT29/ID-VV+VSV* – HT29 cell tumour growth under VV and VSV treatment (administered sequentially) in immune-deficient mouse model
- *4T1/IC* – 4T1 cell tumour growth in immune-competent mouse model
- *4T1/IC-VSV* – 4T1 cell tumour growth under VSV treatment in immune-competent mouse model
- *4T1/IC-VV* – 4T1 cell tumour growth under VV treatment in immune-competent mouse model
- *4T1/IC-VV+VSV* – 4T1 cell tumour growth under VV and VSV treatment (administered sequentially) in immune-competent mouse model

Overview of fitting algorithm for VV and VSV related viral and immune parameters

We conducted a sequential fit of the experimental measurements digitized from Le Boeuf *et al.*[9] and Rausch *et al*.[12] to estimate viral and immune related parameters. At each step of the fitting algorithm, any parameters that were either not being estimated or had not been previously determined, were fixed to the value determined by Cassidy and Craig[2] (Table TS2).

First, tumour growth parameters were obtained by fitting the parameters a_1, a_2 and d_2 by minimizing the square difference between the average tumour growth measurements and the corresponding model simulation from both the HT29 and 4T1 cell lines in immunodeficient mice (i.e. *HT29/ID* and *4T1/ID*). Then, fixing these parameter values for the HT29 tumour growth, we used the VSV and VV and treated HT29 tumour growth measurements in immunodeficient mice (i.e. *HT29/ID-VSV* and *HT29/ID-VV*) to obtain the virus-specific kinetic parameters κ_{VSV}, κ_{VV}, δ_{VSV}, δ_{VV}, $\alpha_{VSV}, \alpha_{VV}$. As mentioned in the main text, we assumed that VV and VSV would have specific infection rates (κ_{VV} and κ_{VSV}), lysis rates (δ_{VV} and δ_{VSV}), and total virions created through lysis (α_{VV} and α_{VSV})[9].

VV inhibits the production of antiviral factors (such as type 1 interferons) that normally decrease the speed of VSV spread through reducing infectivity and affecting viral production[9]. Thus, we assumed for the experiment in nude mice where VV and VSV are administered sequentially (i.e. *HT29/ID-VV+VSV*), VV would first prime the local tumour environment so that VSV's ability to lyse cells was enhanced, hence the name enhancer. Biologically, we assumed that the reduction in the presence of type I IFN allows for more viral replication leading to faster lysing of infected cells[14]. As such, the lysis rate of VSV-infected cells, δ_{VSV}, would increase in the *HT29/ID-VV+VSV* experiment compared to the previous experiment with VSV alone (i.e. *HT29/ID-VSV*). Additionally, since the multiplicity of infection (MOI) for a virus can be affected by the introduction of a second virus, and MOI can have an impact on replication and lytic properties of viruses[15], we assumed that the lysis rate of VSV infected cells may vary between the single injection of VSV alone and VSV injected after VV was already present. We also assumed all other viral kinetic parameters (κ_{VSV}, κ_{VV}, δ_{VV}, α_{VSV} and α_{VV}) would be the same for the combined virus experiment (i.e. *HT29/ID-VV+VSV*) as the individual virus experiments (*HT29/ID-VV* and *HT29/ID-VSV*).

Immune parameters $k_p, k_{s,q}$ and $\Psi_{1/2}$ were next obtained using the 4T1 tumour growth in an immunocompetent model (*4T1/IC*). Then, to fit the 4T1 tumour growth under VV and VSV treatment (i.e. *4T1/IC-VV* and *4T1/IC-VSV*), we hypothesized that the lysis rates of each virus, δ_{VV} and δ_{VSV}, would vary according to the specific cell line (i.e. HT29 vs 4T1) but the virion infection rate, κ_{VV} and

κ_{VSV}, and the lytic virion burst size, α_{VSV} and α_{VV}, would be conserved. This assumption is based on the belief that virion-cell infection rates will not be significantly affected by the underlying tumour cell type and that the lytic virion burst size would primarily depend on the virus type as opposed to the cell-type. This assumption is supported by observed differences in the length of the eclipse phase for VV (8-10 hours[16]) and VSV (~3 hours[17]), their rates of plaque generation, and overall viral loads[9,18]. The *4T1/IC-VV* and *4T1/IC-VSV* experiments were also used to fit the virion decay rates, ω_{VSV} and ω_{VV}, as we expected these rates to be higher after injection into an immunocompetent mouse.

Since VV reduces the production of antiviral factors[9], we fixed $\rho = 0$ to simulate an anti-inflammatory response was initiated when VV was introduced, and allowed $\rho = 1$ for VSV to reflect its inflammatory properties when administered without VV[9]. In the immunocompetent mouse model where VV and VSV were administered sequentially (*4T1/IC-VV+VSV*), we also assumed that the injection of VSV after VV commenced replication would decrease the maximal immune cell production rate k_{cp}. As elevated cytokine production would increase phagocytosis of cells, ultimately reducing the VSV-infection and subsequent cell lysis, a decrease in k_{cp} would result in an increase in the lysis of VSV-infected cells. To model this effect, we therefore reduced k_{cp}. Additionally, the reduction in immune cell production could be a result of cytokine receptors on virus-specific immune cell binding limited amounts of growth-factors, and competing with newly developing immune cell responses[5] (such as for the VSV infection).

Although the viral kinetic parameters were predominantly estimated using measurement for HT29 tumour growth, we assumed that any impact on viral dynamics of changing to the 4T1 tumour cell line is accounted for by the change in tumour growth parameters between the HT29 and 4T1 cell lines (a_1, a_2, d_2), and also through the variation in lytic burst rate δ_{VSV} and δ_{VV} (Table TS2). In addition, the Le Boeuf et al.[9] experiments measured each virus individually then in combination, providing a more accurate estimation of differences in VV and VSV viral parameters through fitting the tumour growth under either virus individually.

Fig. 1 (Main Text) is a schematic representation of the dynamics occurring in the model for the *4T1/IC-VV+VSV* experiment. Since our model considers only a singular pro-inflammatory cytokine

population and immune compartment, the complex immune network occurring in the VV and VSV treatment had to be simplified. A summary of the fitting procedure for all model parameters is provided in Fig. TS1.

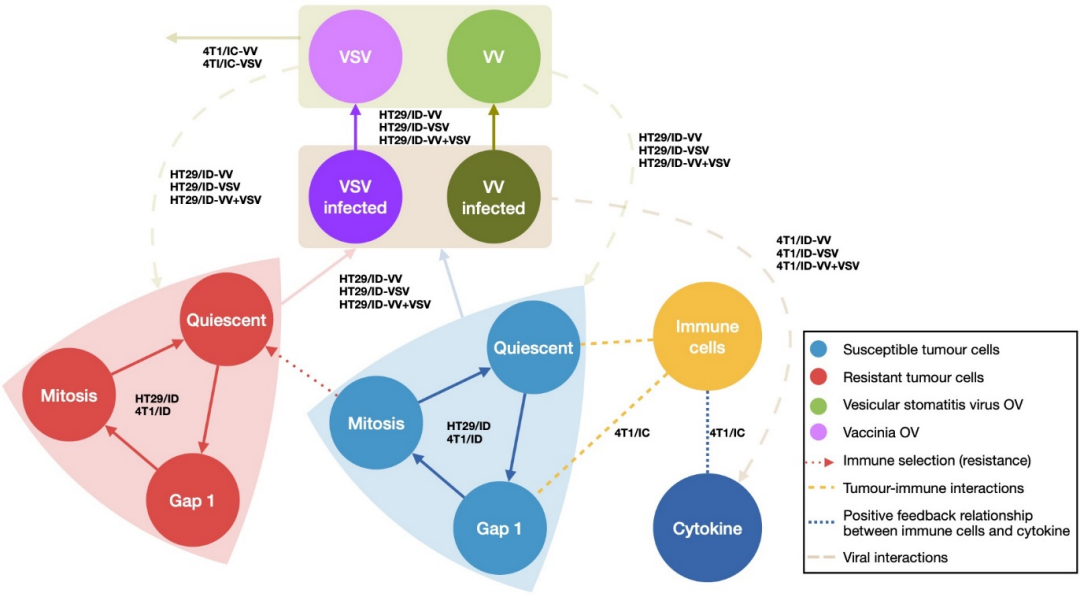

Figure TS1. Hierarchical fitting scheme. *To estimate the parameters in the model, 9 different data sets were used: HT29/ID, HT29/ID-VV, HT29/ID-VSV, HT29/ID-VV+VSV, 4T1/IC, 4T1/IC-VV, 4T1/IC-VSV and 4T1/IC-VV+VSV from Le Boeuf et al.*[9] *and 4T1/ID from Rausch et al.*[12]. *Each of these data sets was used to fit parameters for a specific interaction between the sensitive (blue) and resistant (red) uninfected tumour cells, the sensitive and resistant infected (dark purple and dark green) tumour cells, the virus (dark purple and dark green) and the cytokines (dark blue) and immune cells (yellow). Names of the data set overlaid on the related interaction indicates data sets used to obtain parameters.*

At each step, parameter estimates were obtained by calculating model predictions from the stiff ODE solver *ode15s* in Matlab R2019b and using the nonlinear least squares fitting algorithm *lsqnonlin* via the trust-region-reflective algorithm to estimate parameters that fit model predictions to the data. The termination tolerance was 10^{-6}, the maximum number of function evaluations was fixed as $100 \times$ the number of parameters, and the maximum number of iterations for each fit was 400. Multiple initial seeds were used to confirm that the optimal parameters were obtained. Alternate reduced parameter sets were attempted for the fit of the different data sets, however, the only way to capture the

data was to allow for heterogeneity in the tumour-virus interactions as described in detail above and summarized in Table TS2.

SUPPLEMENTAL RESULTS

Parameter estimates

The initial number of cells for each model simulation was fixed to the corresponding value used in the experiment, or the extrapolation from a $10mm^2$ area to volume, as described above. The values of a_1, a_2 and d_2 for *HT29/ID* and *4T1/ID* tumours were then fitted, with a lower bound for a_2 obtained based on the intermitotic time for cervical cancer cells and the observation that the mean duration of phases S-G_2-M is strictly positive[2], i.e. $\tau = 1.40 - 1/a_2$ and $\tau > 0$. As these mice were immunodeficient, the immune response was ignored and we set $Q_R(t) = G_{1,R}(t) = N_R(t) = P(t) = C(t) = 0$. Additionally, as there was no virus present in the control experiments, $I(t) = V(t) = 0$ (see Fig. TS2A and TS2B, and Tables TS2 and TS3).

Fixing the HT29 tumour growth parameters for the immunodeficient mouse model, the viral-kinetic parameters were obtained by fitting to the *HT29/ID-VV* and *HT29/ID-VSV* experiments, where at $t = 11$ days, a single dose of either VV or VSV was administered. The size of the virus injection was scaled by 10^5 to avoid any computational stiffness of the model. For the dual-dose experiment *HT29/ID-VV+VSV*, VSV was administered two days after the initial dose of VV. As these experiments were also conducted in nude mice, the immune response was negligible, i.e. $Q_R(t) = G_{1,R}(t) = N_R(t) = C(t) = P(t) = 0$. The *HT29/ID-VV*, *HT29/ID-VSV* and *HT29/ID-VV+VSV* experiments were fit simultaneously (see Jenner *et al*.[13] for more details on simultaneously fitting). The results of these fits are provided in Fig. TS2C-TS2E and Tables TS2 and TS3.

Fixing the 4T1 tumour growth parameters obtained for *4T1/ID*, the *4T1/IC* measurements, we next estimated the immune kinetic parameters $k_p, k_{q,s}$ and $\Psi_{1/2}$ (Fig. TS2F and Table TS2). The virus was then recalibrated to the 4T1 tumour cells and the immune presence by fitting $\delta_{VV}, \delta_{VSV}, \omega_{VV}$ and ω_{VSV} to the *4T1/IC-VV* and *4T1/IC-VSV* experiments (Fig. TS2G and TSH). The immune modulation

parameter ρ was fixed to represent the inflammatory and anti-inflammatory capabilities of VV and VSV, respectively.

As discussed above, we hypothesized in the *HT29/ID-VV+VSV* model that the synergism between VV and VSV would alter the lysis rate of the secondary virus (VSV), and we kept this assumption for the immunocompetent equivalent experiment. We also assumed that the injection of VSV into a tumour immune-competent environment after VV commenced replication would further down-regulate the phagocyte production by cytokines at the tumour site, increasing the lysis rate of VSV particles in turn. Therefore, we introduced the piecewise conditions:

$$\rho = \begin{cases} 1 & t < N_E - 1 \\ 0 & N_E - 1 \leq t < N_E - 1 + D_B \\ p^* & t \geq N_E - 1 + D_B \end{cases}$$

and

$$k_{cp} = \begin{cases} k_{cp} & t < N_E - 1 + D_B \\ k_{cp}^* & t \geq N_E - 1 + D_B \end{cases}$$

where N_E is the number of injections given daily (so $N_E - 1$ is the day the last enhancer is administered), and D_B is the lag (days) between the last VV injection and first VSV administration. We then estimated k_{cp}^*, ρ^* and δ_{VSV} by fitting the *4T1/IC-VV+VSV* data (see Fig. TS2I and Table TS2 & TS3).

Overall, the model was able to produce qualitatively what was observed in the data with some minor exceptions. For the HT29 tumour model, initial growth measurements follow an extremely non-linear growth curve, which we were unable to capture exactly. The model dynamics exhibited in the *4T1/IC-VV+VSV* experiment are provided in Fig. TS3. From these estimates, we generated virtual individuals as described in the Main Text by parameterizing normal distributions around parameters so that 99.7% of patients fell within $[\mu - 3\sigma, \mu + 3\sigma] = [0.5\mathbf{p}, 1.5\mathbf{p}]$, where $\mathbf{p}$ is the vector of fitted parameters.

Param		HT29/ ID	4T1/ ID	HT29/ ID-VSV	HT29/ ID-VV	HT29/ ID-VV+VSV	4T1/ IC	4T1/ IC-VSV	4T1/ IC-VV	4T1/ IC-VV+VSV
a_1		**1.54**	**1.66**	1.54	1.54	1.54	1.66	1.66	1.66	1.66
a_2		**1.44**	**1.44**	1.44	1.44	1.44	1.44	1.44	1.44	1.44
d_2		**0.41**	**0.30**	0.41	0.41	0.41	0.30	0.30	0.30	0.30
κ_{VSV}				**0.066**		**0.066**		0.066		0.066
κ_{VV}					**0.054**	**0.054**			0.054	0.054
δ_{VSV}				**5.76**		**29.5**		**1.72**		**11**
δ_{VV}					**18.5**	**18.5**			**2.48**	2.48
α_{VSV}				**1.13**		**1.13**		1.13		1.13
α_{VV}					**1.12**	**1.12**			1.12	1.12
ω_{VSV}				*9.686*		*9.686*		**38.7**		38.7
ω_{VV}					*9.686*	*9.686*			**40.3**	40.3
k_p							**9.23**	9.23	9.23	9.23
$k_{q,s}$							**0.064**	0.064	0.064	0.064
$\Psi_{1/2}$							**1.1×10^{-4}**	1.1×10^{-4}	1.1×10^{-4}	1.1×10^{-4}
k_{cp}	t<8						*4.68*	4.68	4.68	*4.68*
	t>8									**3.08**
ρ	t<6						1	1	1	1
	6<t <8							0		0
	t>8							0		**0.995**

Table TS2. Estimated parameter values. *Parameters in bold are those that were fit to the data set noted by the column. Parameters in italics were values taken from Cassidy and Craig*[2]*. All other parameters were either estimated in a preceding fit and fixed for the resulting fits, or in the case of ρ were fixed to either 0 or 1 based on whether the immune response was upregulated or down regulated. Note that some parameters change with the introduction of the different viruses at t=6 and t=8 and this is labelled in the first column.*

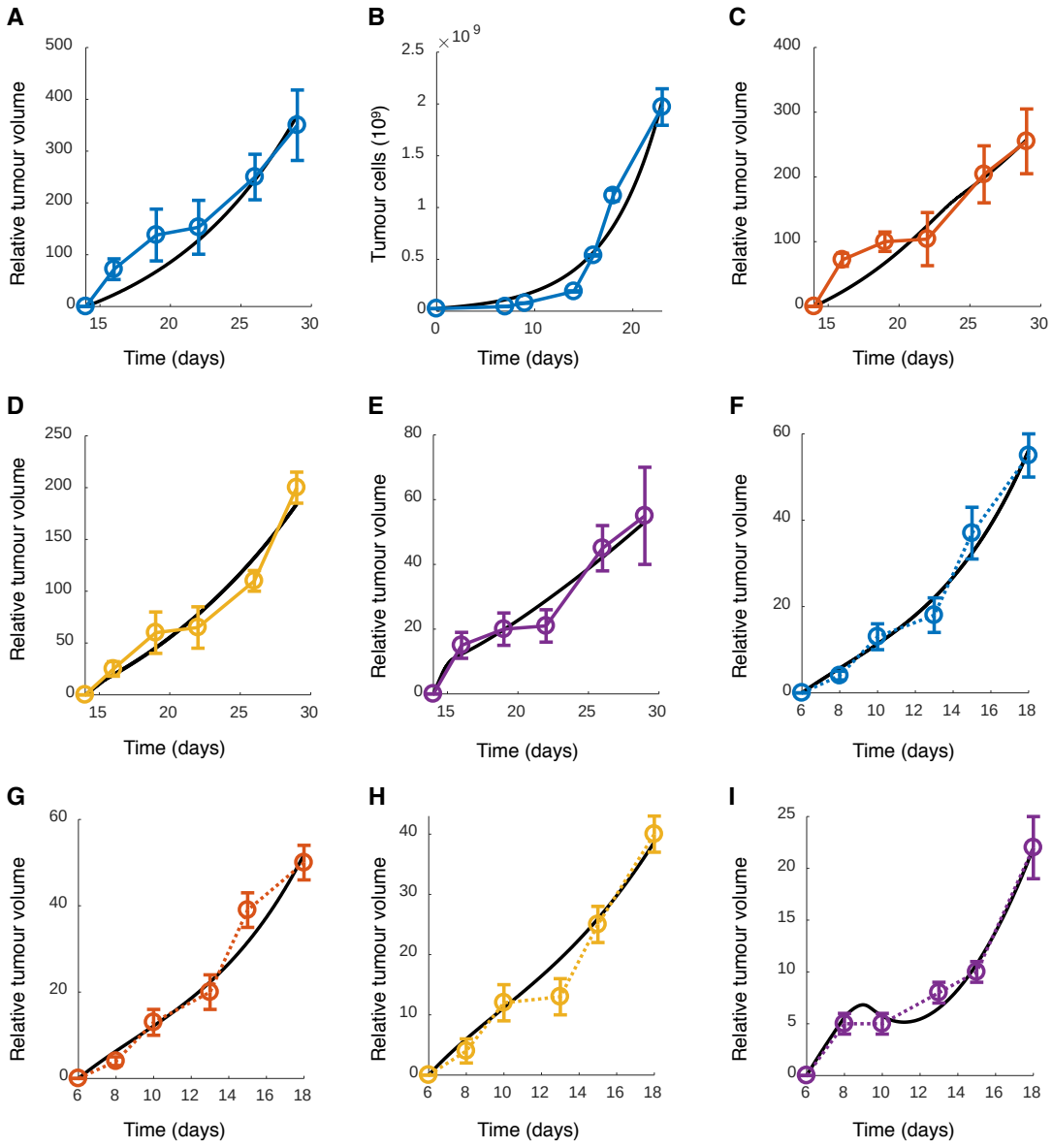

Figure TS2. Parameter estimation results for VV and VSV in immunodeficient and immunocompetent mouse models. *A) HT29/ID. B) 4T1/ID. C) HT29/ID-VV. D) HT29/ID-VSV. E) HT29/ID-VV+VSV. F) 4T1/IC. G) 4T1/IC-VV. H) 4T1/IC-VSV. I) 4T1/IC-VV+VSV. Data is represented by a coloured line joining circles for each data point. The colour of the line corresponds to whether the injection was control (blue), VV (orange), VSV (yellow) or VV+VSV (purple) for immunodeficient animals (solid data lines) or immune-competent animals (dotted data lines), with model predictions overlaid in black solid. Bars on each data point represent standard deviation.*

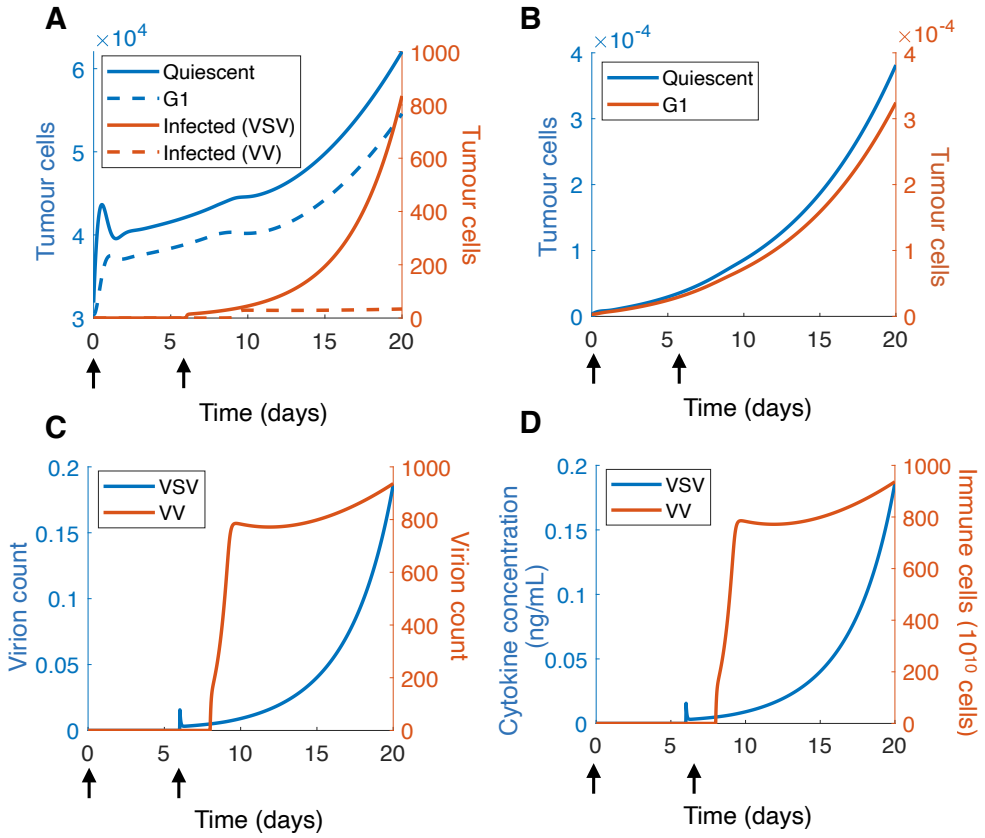

Figure TS3. Model dynamics for the 4T1/IC-VV+VSV model. *A) Number of cells in the Quiescent, G_1, VSV infected and VV infected populations as a function of time. B) Number of cells in the resistant quiescent and resistant G_1 populations as a function of time. C) Number of virions for the VSV and VV virus populations is plotted. D) Cytokine concentrations and immune cells as a function of time. The colour of the line determines its corresponding left (blue) or right (orange) y-axis. The time of the VV and VSV injections is noted by black arrows.*

Parameter	Units	Description	Value
a_1	1/day	Quiescent to interphase rate	1.66
a_2	1/day	Interphase to active phase rate	1.44
d_2	1/day	Interphase death rate	0.3
κ_{VSV}	1/day	VSV virion infection rate	0.066
κ_{VV}	1/day	VV virion infection rate	0.054
δ_{VSV}	1/day	VSV lysis rate	11
δ_{VV}	1/day	VV lysis rate	2.48
α_{VSV}	Virions/cell	VSV burst size	1.13
α_{VV}	Virions/cell	VV burst size	1.12
ω_{VSV}	1/day	VSV virion death rate	38.7
ω_{VV}	1/day	VV virion death rate	40.3
k_p	1/day	Phagocyte-tumour cell contact rate	9.23
$k_{q,s}$	-	Phagocyte cell digestion constant	0.064
$\Psi_{1/2}$	10^{10}cells/day	Cytokine production half effect	0.00011
k_{cp}	10^{10}cells/day	Maximal immune cell production rate	4.68 or 3.08
ρ	-	Immunomodulation constant	0 or 1

Table TS3. Mean parameter estimates used to generate the in silico individuals to investigate perturbations on the combination OV-therapy protocol using the 4T1/IC-VV+VSV model.

Parameter values were obtained from fitting the tumour growth measurements of Le Boeuf et al.[9] *and Rausch et al.*[12] *see Fig. TS3.*

Parameter	Units	Description	Value
d_1	1/day	Quiescent death rate	0
$\hat{d}_g$	1/day	Active phase death rate	0.167
$\eta_{1/2}$	Virions	Virion half effect concentration	0.51
$C_{1/2}$	ng/mL/day	Phagocyte production half effect	0.739
γ_p	1/day	Phagocyte death rate	0.35
C^*_{prod}	ng/mL/day	Homeostatic cytokine production rate	3.9210^{-4}
C^{max}_{prod}	ng/mL/day	Maximal cytokine production rate	1.429
k_{elim}	1/day	Cytokine elimination rate	0.16139
j	-	Number of transit compartments	9
k_{tr}	1/day	Transit rate	10.77
τ	-	Expected cell cycle duration	0.8354
μ	-	Proportion of resistant cells produced	10^{-10}
k^v_a	1/day	Virus absorption rate	20

Table TS4. Mean parameter estimates used to generate the in silico individuals to investigate perturbations on the combination OV-therapy protocol using the results from Cassidy and Craig[2]**.** *For a more detailed description of the parameters see Cassidy and Craig*[2] *or Cassidy and Humphries*[1].

Determination of cumulative survival threshold

The cumulative survival Kaplan-Meier curves generated by Le Boeuf *et al.*[9] for their *4T1/IC-VV+VSV* model was used to determine a culling threshold for the mice cohorts in our virtual trial simulations. Le Boeuf *et al.* measured the proportion of mice with tumours below a certain threshold T^* alive from day 18 to day 40 after an injection of VV on day 6 and VSV on day 8 in 10 different mice (Fig. TS4). To recapitulate the observed survival, we randomly generated 50 cohorts with 10 different mice with mean tumour volume from the fitted curve for the *4T1/IC-VV+VSV* model in Table TS3 and Fig. TS2F. We then simulated tumour growth from day 18 to 40, and used a genetic algorithm to determine that value of T^* that lowered the residual between the cohorts we had generated, and the mice cohorts used by Le Boeuf *et al.* From this procedure, we found $T^* = 246{,}280$ cells.

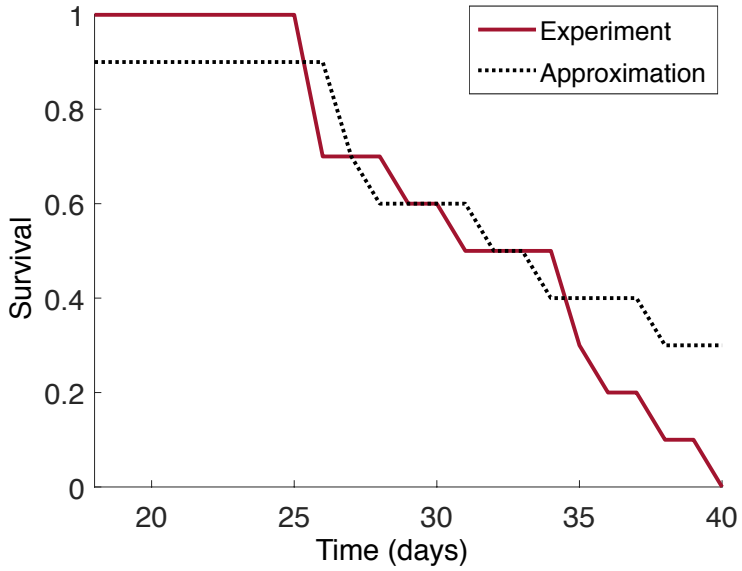

Figure TS4. Comparison of cumulative survival thresholds*. Tumour size of mice at the culling threshold from results reported in Le Boeuf et al.*[9] *4T1/IC-VV+VSV (maroon solid line) was approximated using our virtual trial and applied a genetic algorithm for 10 virtual mice (dotted line).*

Our algorithm would underestimate the tumour culling threshold if mice died prematurely to the threshold set by Le Boeuf *et al.*'s experiments, which could explain the discordance between our generated survival curves and the experimental data. Alternatively, the tumour aggressivity of the mice cohort could be varied differently to our virtual mice cohort, and this would result in a deviation of the cumulative survival curves. Either way, the survival curve approximation from our simulation shows

qualitatively similar behavior and we use this culling threshold T^* in the calculation of the Kaplan Meier survival curves.

REFERENCES

1 Cassidy T, Humphries AR. A mathematical model of viral oncology as an immuno-oncology instigator. *Math Med Biol* 2020;**37**:117–151. doi:https://doi.org/10.1093/imammb/dqz008

2 Cassidy T, Craig M. Determinants of combination GM-CSF immunotherapy and oncolytic virotherapy success identified through in silico treatment personalization. *PLoS Comput Biol* 2019;**15**. doi:10.1371/journal.pcbi.1007495

3 Cassidy T, Craig M, Humphries AR. Equivalences between age structured models and state dependent distributed delay differential equations. *Mathet Biosci Eng* 2019;**16**:5419–50.

4 Jenner A, Yun C-O, Yoon A, *et al.* Modelling heterogeneity in viral-tumour dynamics: The effects of gene-attenuation on viral characteristics. *J Theor Biol* 2018;**454**. doi:10.1016/j.jtbi.2018.05.030

5 Marshall HD, Urban SL, Welsh RM. Virus-induced transient immune suppression and the inhibition of T cell proliferation by type I interferon. *J Virol* 2011;**85**:5929–39.

6 Janeway Jr. CA, Travers P, Walport M, *et al. Immunobiology : the immune system in health and disease*. 6th ed. New York, NY: : Garland Science Publishing 2005.

7 Murray PR, Rosenthal KS, Pfaller MA. *Medical microbiology*. Elsevier Health Sciences 2015.

8 Lee S, Margolin K. Cytokines in cancer immunotherapy. *Cancers (Basel)* 2011;**3**:3856–93.

9 Le Boeuf F, Diallo JS, McCart JA, *et al.* Synergistic interaction between oncolytic viruses augments tumor killing. *Mol Ther* 2010;**18**:888–95. doi:10.1038/mt.2010.44

10 Telfer MG, Preston C, Rothery P. A general method for measuring relative change in range size from biological atlas data. *Biol Conserv* 2002;**107**:99–109.

11 Phelps VR. Relative index finger length as a sex-influenced trait in man. *Am J Hum Genet* 1952;**4**:1952.

12 Rausch MP, Hahn T, Ramanathapuram L, *et al.* An orally active small molecule TGF-β receptor I antagonist inhibits the growth of metastatic murine breast cancer. *Anticancer Res* 2009;**29**:2099–109.

13 Jenner ALAL, Yun COC-O, Kim PSPS, *et al.* Mathematical Modelling of the Interaction Between Cancer Cells and an Oncolytic Virus: Insights into the Effects of Treatment Protocols. *Bull Math Biol* 2018;**80**:1615–29. doi:10.1007/s11538-018-0424-4

14 Sadler AJ, Williams BRG. Interferon-inducible antiviral effectors. *Nat Rev Immunol* 2008;**8**:559–68.

15 Brown CM, Bidle KD. Attenuation of virus production at high multiplicities of infection in Aureococcus anophagefferens. *Virology* 2014;**466**:71–81.

16 Furness G, Youngner JS. One-step growth curves for vaccinia virus in cultures of monkey kidney cells. *Virology* 1959;**9**:386–95.

17 van den Pol AN, Davis JN. Highly attenuated recombinant vesicular stomatitis virus VSV-12′ GFP displays immunogenic and oncolytic activity. *J Virol* 2013;**87**:1019–34.

18 Le-Trilling VTK, Megger DA, Katschinski B, *et al.* Broad and potent antiviral activity of the

NAE inhibitor MLN4924. *Sci Rep* 2016;**6**:1–14. doi:10.1038/srep19977